New Journal of Physics

The open access journal at the forefront of physics

PAPER

CrossMark

Target surface area effects on hot electron dynamics from high intensity laser–plasma interactions

C Zulick, A Raymond, A McKelvey, V Chvykov, A Maksimchuk, A G R Thomas, L Willingale, V Yanovsky and K Krushelnick

Center for Ultrafast Optical Science, University of Michigan, Ann Arbor, MI 48109-2099, USA

E-mail: czulick@umich.edu

Abstract

Reduced surface area targets were studied using an ultra-high intensity femtosecond laser in order to determine the effect of electron sheath field confinement on electron dynamics. X-ray emission due to energetic electrons was imaged using a K_α imaging crystal. Electrons were observed to travel along the surface of wire targets, and were slowed mainly by the induced fields. Targets with reduced surface areas were correlated with increased hot electron densities and proton energies. Hybrid Vlasov–Fokker–Planck simulations demonstrated increased electric sheath field strength in reduced surface area targets.

1. Introduction

Understanding the dynamics of hot electrons from short-pulse laser–matter interactions with solid density targets is important for applications such as fast ignition fusion [1], x-ray and neutron source development [2, 3], ion acceleration [4], warm dense matter [5, 6], and potential medical applications. Hot electrons accelerated during a laser–matter interaction flow along the surface of the target and out into the vacuum, separating from heavier positive ions, and generating strong electromagnetic fields. Such fields have been observed to extend millimeters from the interaction point in foil targets [7]. However, as the electrons spread across the target the hot electron density decreases which reduces the laser conversion efficiency into particle and field energy.

Previous efforts to minimize this effect have primarily focused on small, isolated targets, known as mass limited targets, which increase the hot electron density within the target by decreasing the target volume. In small targets, defined by $2l < c\tau$, where relativistic electrons travel the target thickness, l, and return to the interaction site during the the laser pulse duration, τ, the increased hot electron density is augmented by multiple accelerations of the hot electrons. This process, known as refluxing, has been shown to increase electron [8, 9] and proton energies [10, 11] in thin foils. Studies have also investigated the effect of transverse refluxing in mass limited targets, leading to enhanced fields [12] improved conversion efficiency [13] and enhanced proton energies [14] with laser pulse durations of hundreds of fs. In tens of fs short-pulse interactions it is possible to study the effect of hot electron confinement without refluxing. In this regime, enhanced proton energies in short-pulse interactions have been predicted [15], but have not yet been observed experimentally [16, 17].

While it is straightforward to simulate an isolated, mass limited target, it is quite difficult to reproduce this situation experimentally. To date, approaches have included suspending small targets on glass stalks [5, 18] or ultrathin wires [13], and using micron scale droplets [19–21]. While there are benefits for the use of mass limited targets, they tend to be less practical than simpler traditional targets, such as foils, for applications. Here we investigate the effect of confining the hot electrons through reduced surface area targets without limiting the target mass through isolation or increasing hot electron energies through refluxing.
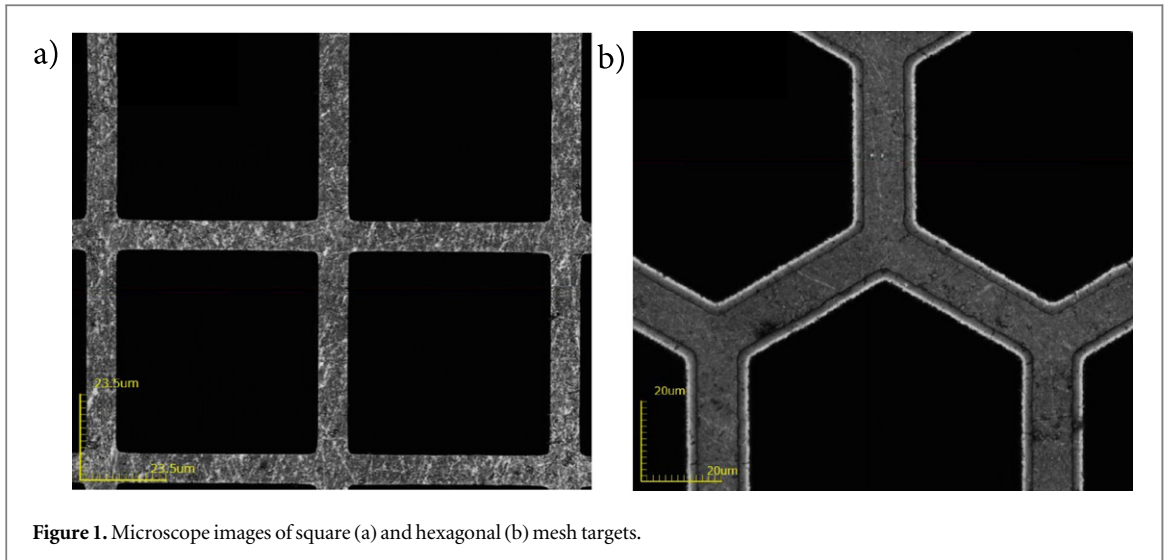
Figure 1. Microscope images of square (a) and hexagonal (b) mesh targets.

2. Methods

The experiment was performed using the HERCULES [22] laser facility at the University of Michigan. HERCULES is a Ti:sapphire system ($\lambda = 800$ nm) which produces $\tau = 40$ fs duration full width at half maximum (FWHM) laser pulses with an amplified spontaneous emission intensity contrast [23] of 10^{-11}. The laser delivered 1.4 (± 0.3) J to the target at normal incidence in a 2.7 μm FWHM focal spot via an $f/3$ off-axis parabolic mirror. This resulted in an average on-target intensity of 6.1×10^{20} W cm^{-2} ($a_0 = 17$). A near diffraction limited spot size with a Strehl ratio of 0.6–0.95 was attained by using a deformable mirror (Xinetics) and a Shack–Hartmann wave front sensor [24]. A comparison data point is shown from the T-cubed laser, which had a longer, 400 fs, pulse duration and lower intensity. The T-cubed laser delivered 7.2 J to the target in a 5 μm FWHM focal spot, which resulted in a focused intensity of 4.5×10^{19} W cm^2 ($a_0 = 5$).
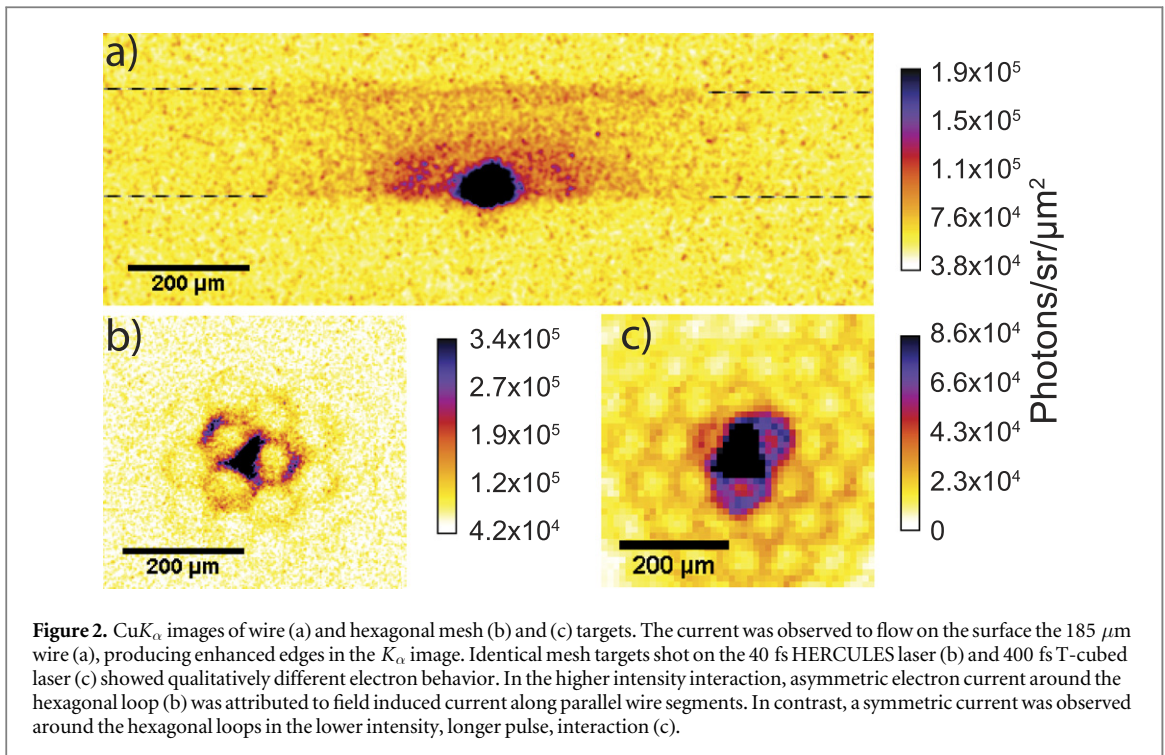
In this letter we present results from foil, mesh, and wire copper targets. The foil target was 12.5 μm thick. The mesh targets were square and hexagonal grids. The square mesh had a 62 μm pitch with 8 μm bar width and was measured to be 9 ± 1 μm thick. The hexagonal mesh had a 83 μm pitch with a 10 μm bar width. Images of the square and hexagonal mesh targets, shown in figure 1, were taken with an Olympus OLS 4000 LEXT laser confocal microscope. The wire target diameters ranged from 15 to 185 μm. The targets were selected to vary the target surface area while maintaining approximately the same target thickness. For a given foil target area, the effective area was reduced by 64% for the mesh target, and 96% for the 15 μm diameter wire. While previous studies have shown increased maximum proton energies with thinner targets [25] and hydrogen-containing targets [26], for this study the target thickness was selected to elucidate the underlying physics by isolating the effects of hot electron confinement from refluxing. Transverse alignment of the mesh and wire targets required few micron precision to overlap the focal spot and the 8 μm width mesh bars. This was accomplished by imaging the location of the focused low energy regenerative amplifier laser seed pulse on the target.

The primary ion diagnostic was CR-39 located normal to the target on the rear side. CR-39 was chosen as the ion diagnostic in order to capture spatial information about the accelerated proton beam. Mylar filter stacks were used to measure proton flux in multiple energy bins, allowing the measurement of a proton energy spectrum. Each bin acted as a high pass filter yielding a proton signal above the energy cut-off. CR-39 was placed at distances of 1 or 5 cm from the target to measure the proton beam profile or 45 cm from the target to measure the energy and flux.

CuK_α emission from the targets was imaged using a spherically bent Quartz (21$\bar{3}$1) crystal with a $2d = 3.082$ Å lattice spacing. The crystal, which had a 400 mm bending radius, was placed 242 mm from the target in the forward, or laser, direction and produced an image at 1260 mm, yielding a magnification of 5.2. An Andor iKon-M BR–DD was used to detect the photons. The imaging system was aberration limited to a resolution of 15 μm at the target with a 25.4 mm crystal aperture. The absolute photon yield was calculated using the manufacturer specified CCD response and crystal's integrated reflectivity.
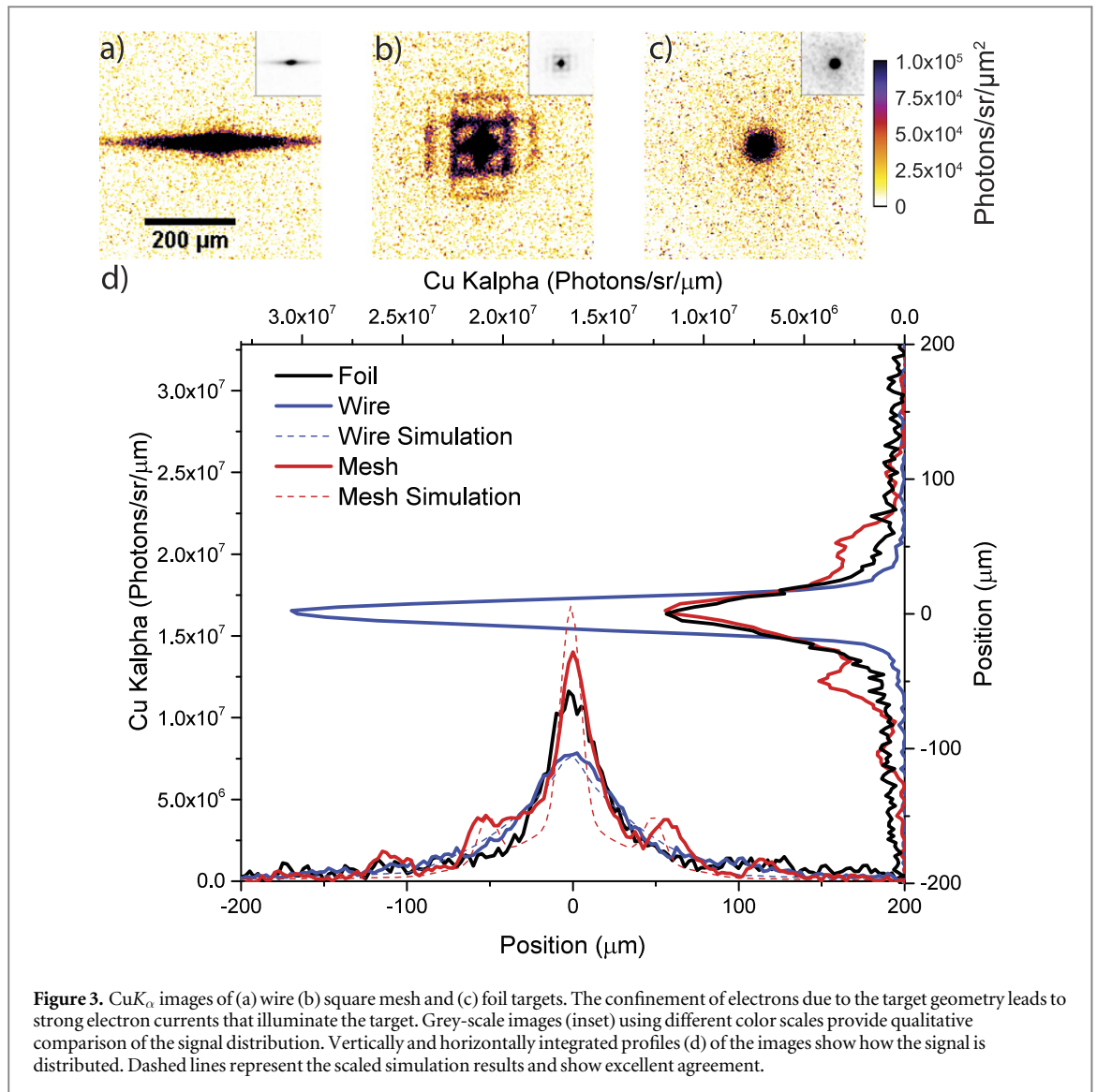
3. Results

The CuK_α images provided insight into the hot electron dynamics by measuring the relative magnitude and location of hot electrons within the target material, as shown in figure 2. Edge-enhancement of the CuK_α signal

Figure 2. CuK_α images of wire (a) and hexagonal mesh (b) and (c) targets. The current was observed to flow on the surface the 185 μm wire (a), producing enhanced edges in the K_α image. Identical mesh targets shot on the 40 fs HERCULES laser (b) and 400 fs T-cubed laser (c) showed qualitatively different electron behavior. In the higher intensity interaction, asymmetric electron current around the hexagonal loop (b) was attributed to field induced current along parallel wire segments. In contrast, a symmetric current was observed around the hexagonal loops in the lower intensity, longer pulse, interaction (c).

in figure 2(a) demonstrated that the current was flowing on the surface of the 185 μm wire. This provided experimental corroboration of simulations of laser induced electron transport in 40 μm wires which predict that the bulk of the current traveled along the wire surface [27].

In figures 2(b) and (c) the CuK_α signal from identical hexagonal mesh targets showed distinct differences between the HERCULES (b) and T-cubed (c) shots. The higher intensity HERCULES shot showed an asymmetry, as the current is traced along hexagonal loops, with an enhancement of the current in wire segments parallel to the wire segment at the laser focus. Alternatively, the lower intensity and longer pulse duration T-cubed shot showed uniform current flow along the segments of the hexagons. The illumination of parallel wire segments in HERCULES shots was also observed using square mesh targets, as pictured in figure 3 (b), and was observed to be independent of laser polarization. The higher intensity HERUCLES interaction produced 4.2 times higher photons sr^{-1} μm^{-2} in the parallel mesh segments than the T-cubed interaction, despite the lower energy. This suggested that the lower intensity interaction of T-cubed drove a direct current in the target, while the higher intensity of HERCULES drove a much higher peak current of hot electrons which induced current in parallel wires through strong electric and magnetic field growth. In the HERCULES shots it was observed that the magnitude of the enhanced signal in parallel wire segments decreased as $1/r^{1.3}$, where r was the distance from the laser interaction. This was consistent with an induced current resulting from the growth and decay of a magnetic field of the form $B(t, r) \approx I(t)/r$. Alternatively, direct current would be expected to scale exponentially, while an expanding plasma could be expected to scale as $1/r^2$. It is of interest to note that while the higher energy of the T-cubed laser led to CuK_α illumination of a larger extent of the hexagonal mesh, the HERCULES and T-Cubed shots had similar conversion efficiencies, and the photon flux per Joule was found to be 1.1×10^9 and 1.3×10^9 photons sr^{-1} J^{-1}, respectively.
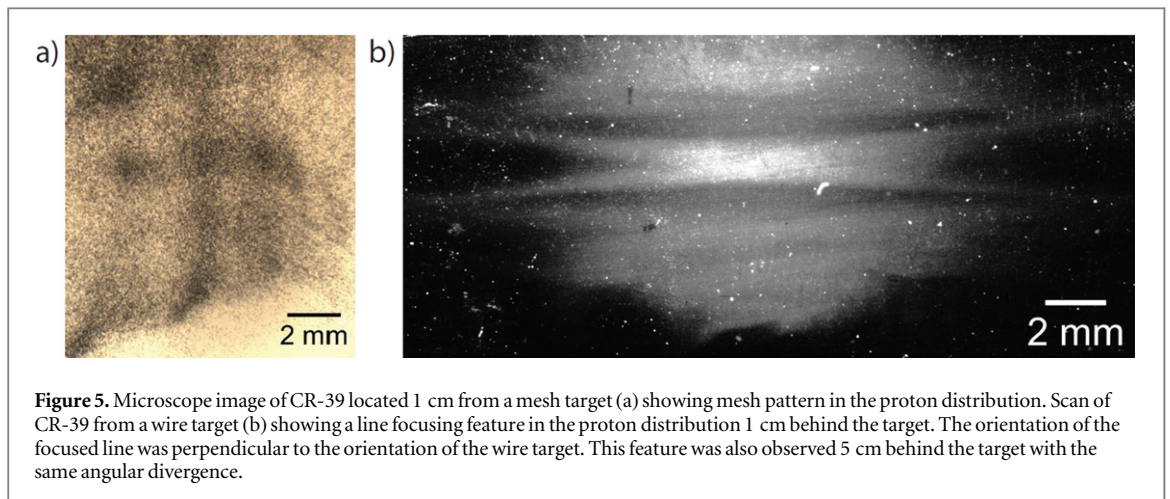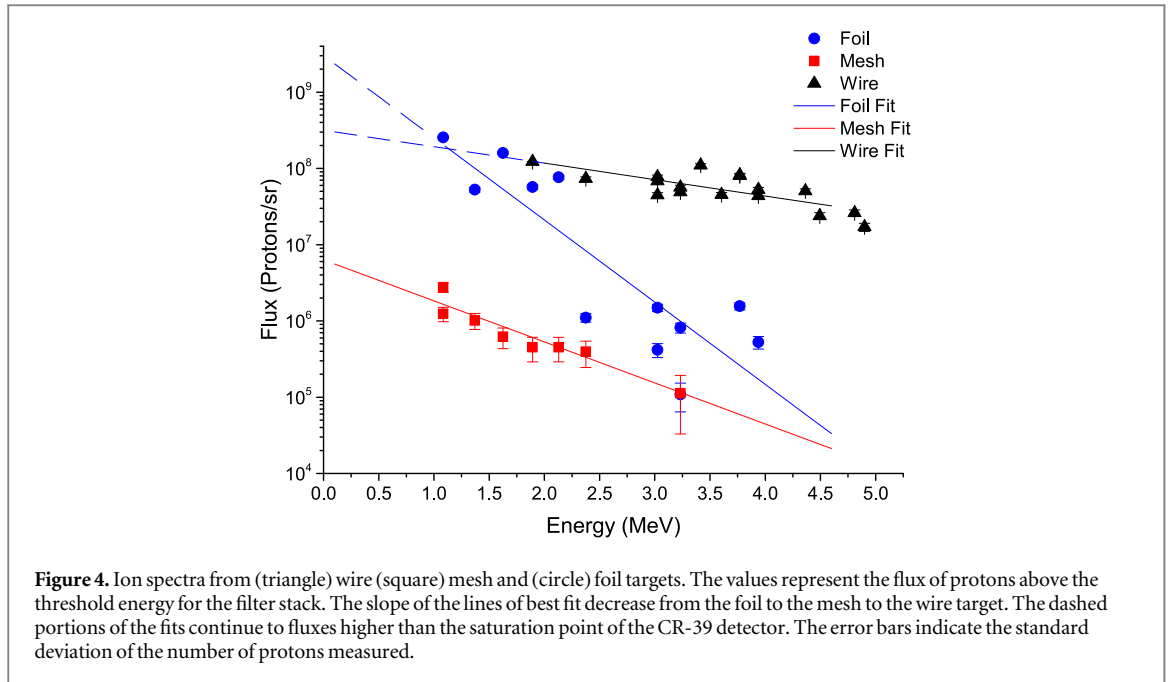
The effect of limiting the target surface area on electron dynamics was measured using foil, mesh, and 15 μm wire targets on HERCULES, as shown in 3(a)–(c). The total CuK_α flux was remarkably consistent between targets, varying from 9.5×10^9 to 1.1×10^{10} photons in the three images in figure 3, which is consistent with laser shot-to-shot fluctuations. The total laser conversion efficiency into CuK_α was 1×10^{-5}, consistent with previous results [6, 28]. Previous studies have shown a reduction in CuK_α yield for lower volume targets with pulse energies >75 J [29, 30], which was partially attributed to broadening and shifting of the K_α emission as a result of heating. A reduced K_α signal was not observed for lower volume targets investigated here, indicating the target heating was insufficient to alter the K_α emission. While the total K_α flux was consistent, the spatial distribution of the signal was confined to the target. The vertical and horizontal profiles (d) of the K_α images showed enhanced signal in the vertical profile of the wire signal and along the mesh segments. This showed that confinement of the electrons in the reduced surface area targets led to increased hot electron density. The horizontal profiles of the wire and foil were similar since the electron flow was unrestricted in the horizontal direction in these targets.

Figure 3. CuK_α images of (a) wire (b) square mesh and (c) foil targets. The confinement of electrons due to the target geometry leads to strong electron currents that illuminate the target. Grey-scale images (inset) using different color scales provide qualitative comparison of the signal distribution. Vertically and horizontally integrated profiles (d) of the images show how the signal is distributed. Dashed lines represent the scaled simulation results and show excellent agreement.

The K_α images also provided information about the mechanism by which electrons lost energy in the target. The extent of the horizontal K_α profile was observed to be similar for all three targets, despite the variations in target areal density. This indicated that the electrons primarily lost energy to, and were confined by, the induced fields, as opposed to collisions within the target. The relative importance of the induced fields in the hot electron confinement was emphasized in the reduced surface area targets, where increased hot electron densities were observed despite reduced energy loss from collisions due to the lower areal density.

The effect of the increased hot electron density on the sheath field was investigated by measuring the proton spectra, which provided a direct measurement of the sheath field. The proton spectra, shown in figure 4, were well characterized by exponential fits. The lines of best fit, in units of protons sr^{-1}, were $Y_{foil} = 3.0 \times 10^9 \times e^{-E/0.40}$, $Y_{mesh} = 6.3 \times 10^6 \times e^{-E/0.81}$, and $Y_{wire} = 3.2 \times 10^8 \times e^{-E/2.0}$, where E was the energy of the protons in MeV. The effective temperature of the spectra increased as the target surface area was reduced from the foil to the mesh to the wire. This result indicated that as the electron sheath was confined to a smaller area the field strength increased, accelerating protons to higher energies.

While the effective temperature demonstrated a clear trend, the total proton flux did not. As the surface area of the target decreased it was expected that the area from which protons were accelerated would also decrease, and thus the number of protons would decrease. While a reduced proton flux was observed for the mesh, the wire target had nearly the same flux as the foil. This was attributed to a focusing feature observed in the proton spatial distribution, as shown in figure 5(b). The line focused protons were observed 1 and 5 cm from the target, with the same 7° full-width-full-angle vertical divergence. This focused divergence was considerably smaller than the full beam 54° full-width-full-angle divergence for the protons that were not focused. It was also much smaller than the 40° full-width-full-angle proton beam observed from flat targets. The focused protons were sampled for the energy spectra.

Figure 4. Ion spectra from (triangle) wire (square) mesh and (circle) foil targets. The values represent the flux of protons above the threshold energy for the filter stack. The slope of the lines of best fit decrease from the foil to the mesh to the wire target. The dashed portions of the fits continue to fluxes higher than the saturation point of the CR-39 detector. The error bars indicate the standard deviation of the number of protons measured.

Figure 5. Microscope image of CR-39 located 1 cm from a mesh target (a) showing mesh pattern in the proton distribution. Scan of CR-39 from a wire target (b) showing a line focusing feature in the proton distribution 1 cm behind the target. The orientation of the focused line was perpendicular to the orientation of the wire target. This feature was also observed 5 cm behind the target with the same angular divergence.

The profile of the protons accelerated from the square mesh target was also interesting. The target mesh pattern was observed in the proton flux on CR-39 placed 1 cm behind the target, as shown in figure 5(a). Three vertical lines and four horizontal lines are evident in the proton distribution. This image confirmed that the electrons that produced CuK_α on neighboring segments of mesh around the focal spot also generated sheath fields which accelerated protons. Furthermore, it confirmed that the extent of the CuK_α signal was approximately the extent of the sheath field that contributed to proton acceleration. Additionally, this correlation between the extent of the sheath field and CuK_α signal was observed in simulations.

4. Simulations

To help understand the experimental results simulations were performed for the wire and mesh target geometries using the hybrid Vlasov–Fokker–Planck code, FIDO [31]. Excitation of K shell vacancies was calculated from collisions between the fast electron population and the background fluid [32]. The simulation domain consisted of a box of dimensions $L_y = 100$ μm by $L_x = 200$ μm in an (x, y) 2D slab geometry with a grid spacing of 2.5 μm in both directions. The copper targets were represented by piecewise hyperbolic tangent functions. The initial temperature of the bulk target was $k_B T_e = 400$ eV. A cut-off was introduced such that $\ln \Lambda_{ei} = 2$ if the calculated value was less than 2. The boundary conditions were reflecting and the last few grid points had an exponentially increasing step size. An isotropic population of electrons was injected into a 5 μm region at the center of the domain with a full width at half maximum temporal duration of 40 fs. The electron
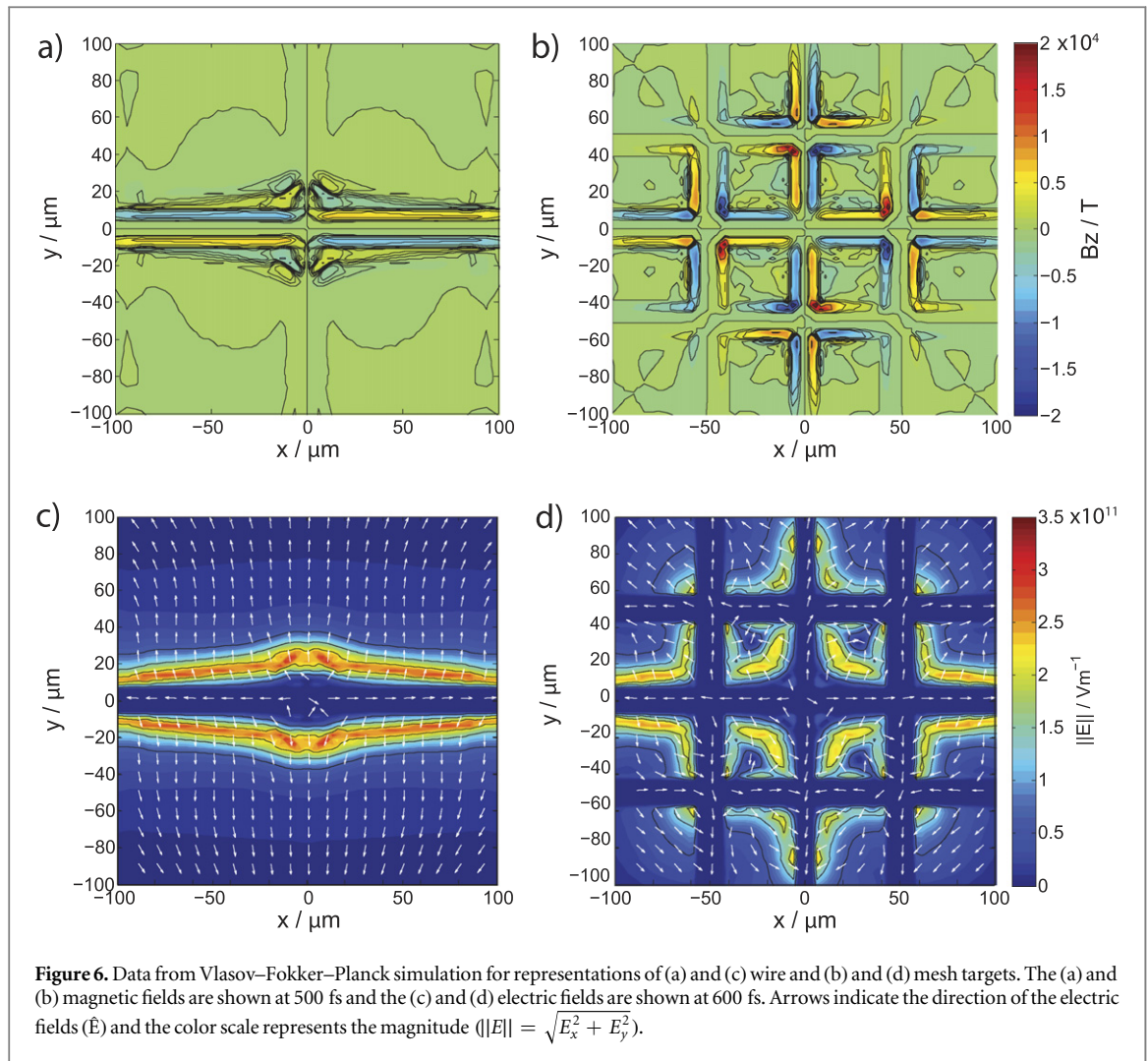
Figure 6. Data from Vlasov–Fokker–Planck simulation for representations of (a) and (c) wire and (b) and (d) mesh targets. The (a) and (b) magnetic fields are shown at 500 fs and the (c) and (d) electric fields are shown at 600 fs. Arrows indicate the direction of the electric fields (Ê) and the color scale represents the magnitude ($||E|| = \sqrt{E_x^2 + E_y^2}$).

beam momentum distribution was defined as in [31] with p as a shifted Gaussian with center momentum $p_0 = (\sqrt{1 + a_0^2} - 1)2m_e c^2/3$ [33]. a_0 was chosen to be representative of a laser with an intensity of 2×10^{19} W cm^{-2}, but with a larger focal area in order to match the laser energy from the experiment, with the injected electron beam number density being calculated using the effective laser energy with an assumed 0.3 absorption fraction.

An azimuthal magnetic field was observed around the wire target, as seen in figure 6 (a). The field switched orientations around the interaction point due to the change in current directions. This field geometry was consistent with the observed proton focusing. In the grid target azimuthal fields were also observed (b). However, the crossing segments broke up the collective focusing structure.

The spatial extent of the fields was observed to be consistent between the wire and the mesh, as observed experimentally. The wire target electric field strength, shown in figure 6 (c), peaked at 2.9×10^{11} V m^{-1} while the mesh target maximum, shown in figure 6 (d), was only 2.2×10^{11} V m^{-1}. The higher wire field strength was consistent with the experimentally observed wire proton temperature increase. The electric field structure also provided insight into the different proton fluxes observed from the two targets. The laminar field structure around the wire target led to efficient acceleration of protons. Conversely, the low proton flux from the grid targets could be partially attributed to the complex field structure, around the intersection points, which could accelerate protons in a wider divergence angle than the other two targets.

5. Conclusions

In conclusion, hot electron dynamics have been studied using structured targets with reduced surface areas. Reduced surface area targets were observed to confine hot electrons to higher densities through induced fields. A comparison between the HERCULES and T-cubed shots suggested the higher intensity interaction led to field-induced current which resulted in the observed K_α asymmetry. This result illustrates how the dynamics of

femtosecond laser produced hot electrons are fundamentally different from picosecond sources. Additionally, the observation of a field-induced current could be important in high intensity interactions with complex target geometries such as a fast ignition entrance cone.

Proton focusing was observed with the wire target, which simulations showed, was the result of azimuthal magnetic fields resulting from the surface current. The mesh target profile was imprinted on the proton profile. Focused proton beams and imprinted beam profiles could be utilized to tailor a beam profile to an application.

The hot electron density was observed to increased as the target surface area was reduced and was correlated to an increase in the sheath field strength, which increased the temperature of the accelerated proton beam. The increase in sheath field strength was also observed in simulations. While these studies were performed on targets that were several microns thick, an increase in hot electron density and proton energy would be expected for reduced surface area versions of traditional thin films [25] and hydrogen-containing target materials [26], which have already been shown to produce 10–20 MeV protons. Enhanced proton energies would also be expected as a result of refluxing in smaller targets. The increased proton energies, without the use of complex mass limited targets, could be used to enhance proton energies without the need for higher energy lasers. The use of targets with reduced surface areas also pairs well with femtosecond lasers which typically achieve high focal intensity through sharp focal optics and few micron scale focal spots.

Acknowledgments

References

[1] Tabak M, Hammer J, Glinsky M E, Kruer W L, Wilks S C, Woodworth J, Campbell E M, Perry M D and Mason R J 1994 *Phys. Plasmas* **1** 1626

[2] Rousse A, Audebert P, Geindre J P, Falliès F, Gauthier J C, Mysyrowicz A, Grillon G and Antonetti A 1994 *Phys. Rev.* E **50** 2200–7

[3] Zulick C *et al* 2013 *Appl. Phys. Lett.* **102** 4101

[4] Wilks S, Langdon A, Cowan T, Roth M, Singh M, Hatchett S, Key M, Pennington D, MacKinnon A and Snavely R 2001 *Phys. Plasmas* **8** 542

[5] Baton S *et al* 2007 *High Energy Density Phys.* **3** 358–64

[6] Neumayer P, Lee H, Offerman D, Shipton E, Kemp A, Kritcher A, Döppner T, Back C and Glenzer S 2009 *High Energy Density Phys.* **5** 244–8

[7] McKenna P *et al* 2007 *Phys. Rev. Lett.* **98** 145001

[8] Chen H and Wilks S 2005 *Laser Part. Beams* **23** 411–6

[9] Quinn M *et al* 2011 *Plasma Phys. Controlled Fusion* **53** 025007

[10] Mackinnon A, Sentoku Y, Patel P, Price D, Hatchett S, Key M, Andersen C, Snavely R and Freeman R 2002 *Phys. Rev. Lett.* **88** 215006

[11] Tresca T *et al* 2011 *Plasma Phys. Controlled Fusion* **53** 105008

[12] Kluge T, Enghardt W, Kraft S, Schramm U, Zeil K, Cowan T and Bussmann M 2010 *Phys. Plasmas* **17** 123103

[13] Morace A *et al* 2013 *Appl. Phys. Lett.* **103** 054102

[14] Buffechoux S *et al* 2010 *Phys. Rev. Lett.* **105** 015005

[15] Limpouch J, Psikal J, Andreev A, Platonov K and Kawata S 2008 *Laser Part. Beams* **26** 225–34

[16] Sokollik T, Schnürer M, Steinke S, Nickles P, Sandner W, Amin M, Toncian T, Willi O and Andreev A 2009 *Phys. Rev. Lett.* **103** 135003

[17] Sokollik T, Paasch-Colberg T, Gorling K, Eichmann U, Schnürer M, Steinke S, Nickles P, Andreev A and Sandner W 2010 *New J. Phys.* **12** 113013

[18] Henig A *et al* 2009 *Phys. Rev. Lett.* **102** 095002

[19] Ter-Avetisyan S, Schnürer M, Nickles P V, Kalashnikov M, Risse E, Sokollik T, Sandner W, Andreev A and Tikhonchuk V 2006 *Phys. Rev. Lett.* **96** 145006

[20] Kemp A J and Ruhl H 2005 *Phys. Plasmas* **12** 033105

[21] Busch S, Schnürer M, Kalashnikov M, Schönnagel H, Stiel H, Nickles P V, Sandner W, Ter-Avetisyan S, Karpov V and Vogt U 2003 *Appl. Phys. Lett.* **82** 3354–6

[22] Bulanov S S *et al* 2008 *Medical Phys.* **35** 1770

[23] Chvykov V, Rousseau P, Reed S, Kalinchenko G and Yanovsky V 2006 *Opt. Lett.* **31** 1456–8

[24] Zulick C A 2014 Radiation generation from ultra intense laser–plasma interactions with solid density plasmas for active interrogation of nuclear materials *PhD Thesis* University of Michigan, Michigan

[25] Dollar F *et al* 2012 *Phys. Rev. Lett.* **108** 175005

[26] Dollar F *et al* 2013 *Appl. Phys. Lett.* **103** 141117

[27] Sawada H, Higginson D P, Link A, Ma T, Wilks S C, McLean H S, Pérez F, Patel P K and Beg F N 2012 *Phys. Plasmas* **19** 103108

[28] Urry M, Gregori G, Landen O, Pak A and Glenzer S 2006 *J. Quant. Spectrosc. Radiat. Transfer* **99** 636–48

[29] Akli K U *et al* 2007 *Phys. Plasmas* **14** 023102

[30] Nilson P M *et al* 2010 *Phys. Rev. Lett.* **105** 235001

[31] Sherlock M 2009 *Phys. Plasmas* **16** 103101

[32] Thomas A, Sherlock M, Kuranz C, Ridgers C and Drake R 2013 *New J. Phys.* **15** 015017

[33] Wilks S, Kruer W, Tabak M and Langdon A 1992 *Phys. Rev. Lett.* **69** 1383